Fatigue Damage Analysis on Body Shell of a Passenger Vehicle

E.S. Palma and F.A.C. Vidal

(Submitted 11 February 2002)

A method for design durability qualification of a vehicle body shell is presented. Field test data were used to produce an accelerated durability test that retains all of the damaging real time load histories present in the original test cycle. Fatigue analysis methods are used to access and compare the fatigue damage imposed during durability test and laboratory (torsion) experiments. A numerical methodology (FEM) was used to determine the critical local stresses on the component. These stresses were then experimentally measured by using strain gauges. Field tests were performed over public road tracks (stone paved and land surfaces) for loaded and empty vehicles in the customer enviroment. This acquired data was used to simulate durability tests in laboratory. A correlation between the results obtained in the durability tests and those obtained in a torsion experiment in laboratory was done.

Keywords cumulative fatigue damage, fatigue life prediction, fatigue simulation

1. Introduction

Fatigue damage has long been an important aspect of designing an automotive component to perform a specific function, and it has been extensively studied.[1-3] Design engineers have to accurately predict the service performance of their components. Among others, fatigue life is one of the most important properties when designing such components. The majority of structural components under actual conditions, in the customer's enviroment, are subjected to random amplitude service loading, during their lives. However, the fatigue strength of alloys and components has conventionally been measured in laboratory, using constant amplitude tests. The fatigue lives for components subjected to variable amplitude loads can be quite below the fatigue life predicted using constant amplitude experiment results.[2-5] Thus, determining the service life of a component can be quite complex due to variations in component geometry, materials, and load histories. The solution on this realistic problem requires assessment of these variable parameters by performing experiments under actual conditions.

Durability tests are made, in most cases, to identify potentially critical locations in a structure and to make fatigue life predictions. In these tests, an assembly or a complete vehicle is subjected to actual service conditions prior to production line scale. A component, thus tested, will prove that it will perform as intended for a prescribed period of time. As product complexity, competition, and customer's expectations increase, manufacturers test their products in the customer's environment on public roads. However, it becomes very expensive to do all these tests in the customer's environment. To reduce costs, much of these durability tests can be brought into the laboratory. Thus, customer service operations could be simulated under controlled conditions in the laboratory, producing an economical basis for fatigue life assessment.[5-7] Consequently, one of the most critical applications of fatigue analysis in vehicle and component simulation tests is the correlation between laboratory experiments and durability tests (reproducing the actual conditions in the customer's environment). This correlation can contribute to a significant cost reduction in product design and development since laboratory testing is faster and less expensive than actual service tests. Thus, this work presents a fatigue damage correlation of a body shell between torsion laboratory experiments and durability tests of a vehicle (a passenger car) under different road surface conditions, for either loaded or empty conditions.

1.1 Body Shell: Fatigue and Accelerated Tests Using Vehicular Simulation

Engineering structural components have critical regions of special interest, which are characterized by great variations in stress conditions. Body vehicle nodes constitute some of these regions. The origin of localized stress concentrations and high strains arise from the difficulty of coupling between welded nodes. As they are junction points between elements having distinct forms or characteristics, they do not allow a gradual variation of rigidity, which would avoid the high gradients of localized stresses.[8]

In the automotive industry, the design of the vehicle body shell is determined by aerodynamic form, associated with habitability, internal visibility, and occupant comfort. To meet these requirements, an extreme reduction in the width of specific nodes of the body shell becomes necessary, causing stress concentration. Besides, this node reduction is only made if the safety conditions for the occupants are met. Among the several nodes of the body shell, only those that play an important role on the mechanical behavior of the vehicle are considered.[8]

Life prediction integrates many different analysis and experimental procedures. The combination of analytical, numeri-

E.S. Palma, Department of Mechanical Engineering, Pontifical Catholic University of Minas Gerais, PUC Minas, Belo Horizonte, Brazil; and **F.A.C. Vidal,** Fiat Automobile SA, Betim, Brazil. Contact e-mail: palma@pucminas.br.

cal, experimental, and simulation routes leads to a sound foundation for successful design. Vehicular simulations are applicable to practically all automotive components. Simulation, together with fatigue analysis methods, constitute an important tool for structural component design. Thus, a comparison between virtual and experimental data can be obtained.[7]

There are several types of laboratory simulations of service loading. The primary reason for programmed fatigue testing is that the tests can be accelerated easily. This can be achieved by removing stress cycle regions that do not cause significant damage on the component. Increasing test frequency can also be done to accelerate the test. The result of this edition is an exceptionally lower time for new components development along with cost reduction.[3,9,10]

To make the durability tests (in the laboratory) closer to actual service conditions, the programmed loading data can be obtained during field tests. These data can be reproduced and reworked in laboratory. Besides that, using cycle counting methods, like the rain flow method, together with cumulative fatigue damage theories, leads to a complete reproduction of several kinds of pavement vehicle condition (loaded or empty) in laboratory. Consequently, several service loading conditions can be simulated.

Once stress and strains are determined, they are converted to damage. This transformation involves damage assessment and damage accumulation, which is done cycle by cycle, by using the Miner's rule.[9-11] The damage fraction D_i can be determined by

$$D_i = \frac{n_i}{N_i} \quad \text{(Eq 1)}$$

where n_i is the number of cycles at stress level S_i, and N_i is the fatigue life at the same stress S_i. Failure is assumed to occur when $\Sigma D_i \geq 1$. The life N at the stress σ has to be determined using S-N-curves.

Usually, the S-N-curves are determined for zero mean stress. Thus, from each determined alternating and mean stress pair, an equivalent alternating stress for zero mean stress ($\sigma_{N(0)}$), corresponding to the same life as the original pair (with a nonzero mean stress), can be calculated by using the Goodmann method[9]:

$$\sigma_{N(0)} = \frac{\sigma_a \sigma_r}{(\sigma_r - \sigma_m)} \quad \text{(Eq 2)}$$

In the above equation σ_a, σ_r, and σ_m are the alternating stress amplitude, the ultimate tensile strength and the mean stress, respectively.

Fatigue under proportional biaxial stresses can be treated with methodology developed for uniaxial loading, since principal directions do not change with time. Equivalent alternating (σ_{Eqa}) and mean (σ_{Eqm}) stresses can be calculated using the Von Misses theory:

$$\sigma_{Eqa} = \sqrt{\sigma_{xa}^2 + \sigma_{ya}^2 - \sigma_{xa}\sigma_{ya} + 3\tau_{xya}^2} \quad \text{(Eq 3)}$$

$$\sigma_{Eqm} = \sqrt{\sigma_{xm}^2 + \sigma_{ym}^2 - \sigma_{xm}\sigma_{ym} + 3\tau_{xym}^2} \quad \text{(Eq 4)}$$

where σ_{xya} and σ_{xym} are, respectively, the alternating and mean normal stresses. τ_{xya} and τ_{xym} are the alternating and mean shear stresses.

There are general empirical relationships between fatigue properties of steel and the monotonic tension and hardness properties. Thus, the S-N-curves can be empirically determined in an approximated way, from the ultimate tensile strength (UTS) of the material (σ_{UTS}). The obtained curves must be corrected by modifying factors such as temperature, surface roughness, size, thermal treatment, superficial hardness, and loading type.[9]

2. Materials and Experimental Methodology

2.1 Finite Element Analysis and Materials

The first step of this work was the stress analysis of the body shell, through computer simulation using finite element method (I-DEAS program). This static analysis was performed to obtain the stresses at critical points. To this purpose, a torque

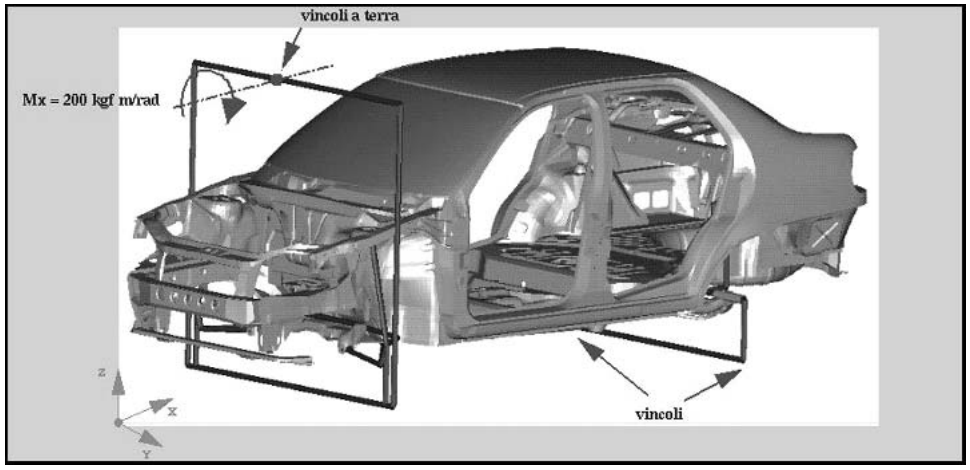

Fig. 1 Torsion test setup to apply a torque in a body shell

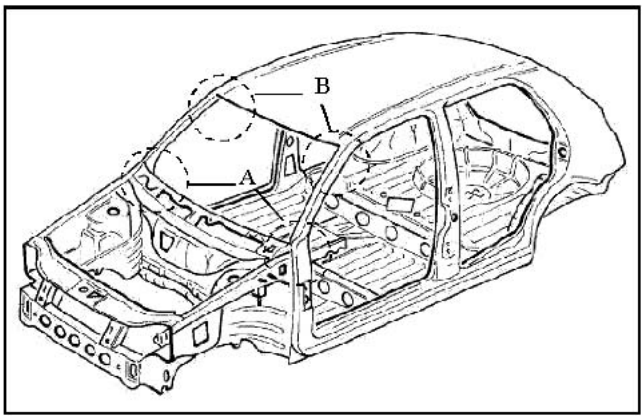

Fig. 2 Region for fixing the sensors

Table 1 Chemical Composition for FEPO4[12]

Element	C	Mn	Al	P	S	Si	N
%	0.006	0.17	0.02	0.017	0.0077	0.017	0.052

Table 2 Mechanical Properties for FEPO4[12]

Ultimate Strength σ_{UTS}, MPa	Yield Limit $\sigma_{0.2}$, MPa	$-\sigma_{0.2}/\sigma_{UTS}$	Elastic Modulus E, GPa	Poisson's Ratio ν
270–350	140–210	0.62	200	0.28

of 200 kgm was applied, using as reference the torsion test setup according to Fig. 1.

The body shell used in this work was made from FEP04 steel (Fiat code), which corresponds to SAE-AIS$_I$ 1005-1009 steel. This steel is also called "EEP steel" because it is used in mechanical parts that require an extra deep drawing. These materials are used with a sheet thickness varying from 0.4-3 mm with extra-low carbon content.

The chemical composition and mechanical properties for the FEP04 steel are shown in Tables 1 and 2, respectively.

2.2 Vehicle Instrumentation

From the results of FEM-analysis, the regions for fixing the sensors were defined, as shown in Fig. 2. They are internal node A and internal node B, both on the driver side and passenger side.

The vehicle instrumentation was done by using HBM (Hottinger Baldwin Messtechnik) electrical strain gauges (rosettes), model 6/120RY11, type 0/45/90° with 120.0 ± 0.5Ω resistance, and gauge factor $K = 2.09$. A rosette fixed at the internal node A on the passenger side is shown in Fig. 3.

In addition to strain gauges, accelerometers and displacement transducers were used for data acquisition during the field tests on public roads. The instrumentation for data acquisition on public road tracks, which were used for the reproduction of the data in the road simulator, are described in Tables 3 and 4.

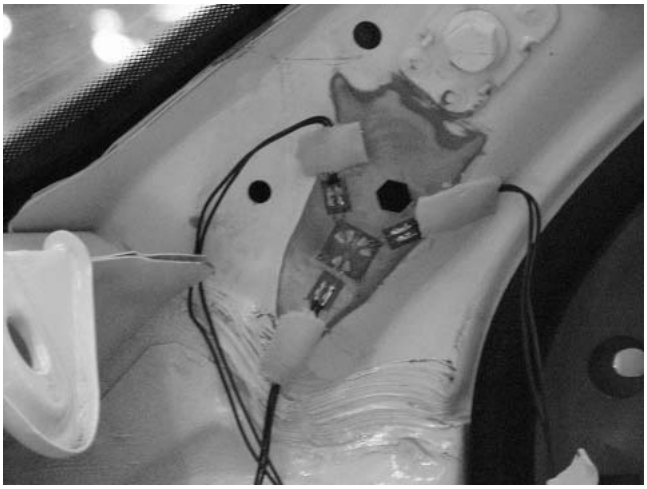

Fig. 3 Rosette fixed at internal node A

Table 3 Accelerometer Data

Equipment Description	Location
Accelerometer, Model 141, Setra ± 60 g	Rear suspension, right side Rear suspension, left side Front damper, right side Front damper, left side
Accelerometer, Model 141, Setra ± 15 g	Front right pillar, damper fixing Front left pillar, damper fixing Rear right pillar, damper fixing Rear left pillar, damper fixing

Table 4 Displacement Transducers Location

Equipment Description	Location
Displacement transducer ASM Model WS1-1-500-R1K-L 10HG	Front right damper Front left damper Rear right wheel
Measurement range: 500 mm	Rear left wheel

2.3 Field Tests on Public Roads In the field test, the vehicle was submitted to the customer enviroment so that multiaxial field data could be collected from accelerometers mounted on suspension and dampers. Subsequently, these data were used to develop a durability test on the simulator. The standard field test route totaled a round trip of 220 km on public roads. These roads were composed of stone pavement (15 km) and unpaved land surface (20 km). The tests were made with empty vehicle Std B (car body weight + driver 70 kg + liquid tanks full) and loaded vehicle Std C (5 passengers = 350 kg + full load condition in the luggauge compartment = 50 kg + liquid tanks full). The acquisition sampling rate was made at 204.8 Hz at a constant vehicle speed of 60 km/h. For each type of pavement and load condition, three runs were made for signal acquisition. The vehicle weights in configurations Std B and Std C are shown in Tables 5 and 6, respectively.

For the reproduction of the collected road data, a road simulator (4-poster), composed of four identical vertical servohy-

draulic actuators, was used. The configuration of this road simulator is shown in Table 7.

To use the road simulator, it is necessary to reproduce the acceleration signals obtained from the road tests in the form of displacements for the actuators. The sequence of these reproduction is shown below (steps 1-5):

1. Transfer, Analysis and Data Edition: In this step, the files generated during the signal acquisition of the road tests are organized. These data are transferred to the computer of the simulator, analyzed, and edited at the stretches, which exceed the displacements limits of the hydraulic actuator (±150mm).
2. System Frequency Response Function (FRF): In this step, the responses of the transducers (accelerometers) are converted to the frequency domain. Thus, the data are stored as displacement amplitudes as a function of frequency. An FRF relationship between the input signal $X(f)$ and the output signal $Y(f)$, perceived by the accelerometers installed at the dampers, is generated. This process originates a matrix of initial correlation $H(f)$. From this matrix, the system generates a function $H^{-1}(f)$, exactly inverse to the initial $H(f)$ and which, multiplied by the output signal $Y(f)$, must be exactly equal to the input signal. $X(f)$[11] This process is shown in Fig. 4.
3. Estimate of the initial signal: At this point the RPC software is in condition to compute the initial signal for the iteration step. If the FRF was a perfect modeling for the signal collected on the road, this would be the last step to be executed. However the FRF is just an approximation of a linear function, in opposite of the road signal, which is completely random. Because of this, it is necessary to correct some differences between the mathematical computational modeling and the road signal. This process is called iteration.
4. Iteration: In this step, the simulator runs the initial iteration signal (drive_0). The output signal (response_0) is sent from the accelerometers to the computer, which is configured to filter values outside of the 0.8–30.2 Hz range. An initial replied signal is thus created. From this point, the input signal is subtracted from the replied signal, creating an error signal (error_0). This is multiplied by the matrix FRF $H^{-1}(f)$ generating a correction signal as function of the displacement (correction_0). Finally, the corrected signal is added to the initial signal, multiplied by the desired gain and sent to the simulator for a new cycle of iteration. Thus a sequence of iterations is created. This process, as shown in Fig. 5, is repeated several times, until the error between the input and output signal resulting from the iterations is lower than 5%. The gain value depends on the precision of the FRF. For highly linear systems, the gain is close to 1, and few iterations are necessary. For highly nonlinear systems, the gain is close to zero and several iterations are necessary. In the case of road signals, the usual gain values vary from 0.4-0.6.
5. Durability Test: After several iterations, the drives are combined and a sequence of block loads is established for the road and loading conditions, and it is used to simulate the durability test. The standard durability test route totalized 12,000 km. This simulation represents a vehicle traveling 8000 km (2/3 of the total) on stone pavement and 4000 km (1/3 of the total) on land surface road (unpaved earth road). Fifty percent of the total test track is done with loaded vehicle condition, and 50% with the empty vehicle condition. The distribution of the durability test is shown in Fig. 6.

Table 5 Empty Vehicle Weight, Standard B

	Left Side		Right Side		Total	
	kgf	Newton	kgf	Newton	kgf	Newton
Front axle	414	4057	394	3860	808	7 917
Rear axle	235	2303	240	2350	475	4 653
Total	649	6360	634	6213	1283	12 573

Table 6 Loaded Vehicle Weight, Standard C

	Left Side		Right Side		Total	
	kgf	Newton	kgf	Newton	kgf	Newton
Front axle	425	4160	410	4020	835	8 180
Rear axle	325	3180	338	3312	663	6 492
Total	750	7340	748	7330	1498	14 670

Table 7 Road Simulator Configuration[13]

Model	MTS 320
Actuators	5.0 KN
Stroke	300 mm
Maximum velocity	1000 mm/s
Maximum acceleration	40 g
Software	458/498 RPCIII

2.4 Torsion Test

The torsion test is performed on a test setup, similar to the one shown in Fig. 1, applying a torque equal to 200 kgm. This value was pre-established in conformity with Fiat test standards, which keep a correlation with the analysis performed with finite element.

The body shell for this test type followed the same structural characteristics of the vehicle used during the durability test. Also, the regions for fixing the rosettes, as well as their technical characteristics, remain the same.

For this test, two configurations of the body shell are used: body-in-white (no doors panels and no windshield glazing) and the complete one (full vehicle body shell). The purpose in

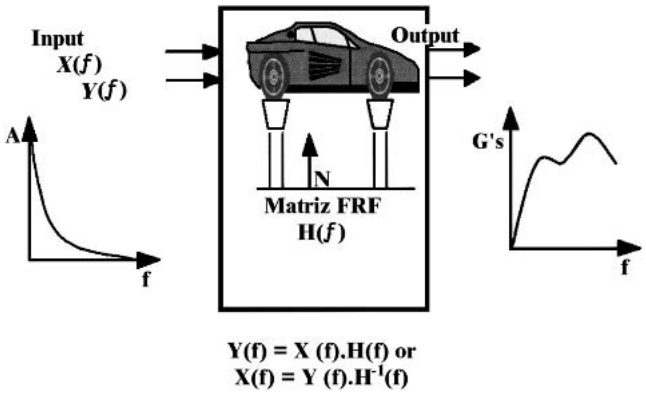

Fig. 4 Measuring the system FRF

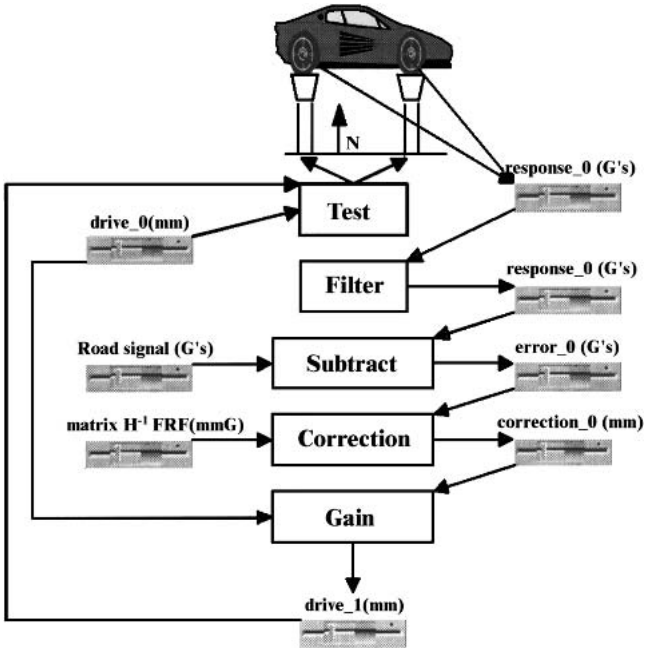

Fig. 5 Iteration cycle

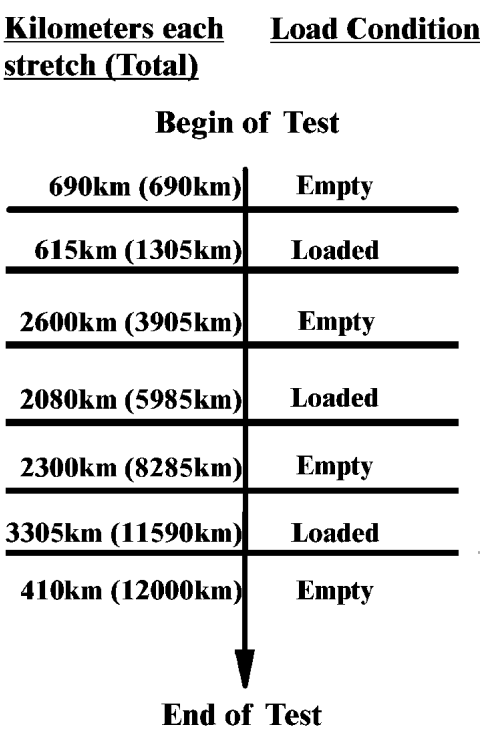

Fig. 6 Distribution of kilometers as a function of the loading condition

using body-in-white is to compare the values obtained by the finite element method with the experimental values. In the case of the complete body shell, the purpose is to reproduce the same configuration of the body of the vehicle tested on the road simulator. The full body shell is different from the tested vehicle in that it does not contain internal and external finishing parts or the motor.

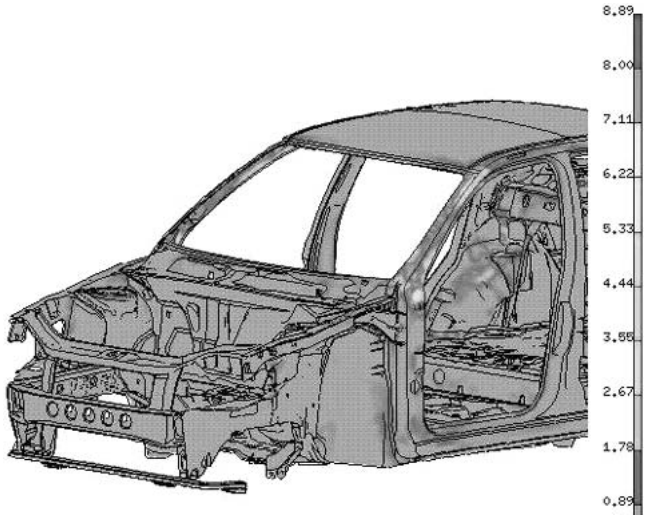

Fig. 7 Finite element analysis results (stresses in kgf/mm^2); note that 1 kgf/mm^2 equals 9.8 MPa.

Table 8 Results of Finite Element Analysis

Location	Von Mises Stress, MPa
Node B, driver side	17.8 a 26.7
Node B, passenger side	17.8 a 26.7
Node A, driver side	35.5 a 44.4
Node A, passenger side	35.5 a 44.4

3. Results

3.1 Finite Element Analysis

Figure 7 shows stress distributions through the front of the body-in-white vehicle shell during application of an input torque equal to 200 kgm by using finite element analysis. The results of this analysis, taking as reference the more stressed regions, are shown in Table 8. These regions are located in vehicle body nodes A and B, as shown in Fig. 7. This stress, however, is not big enough to cause damage on the body shell.

3.2 Reproduction of Signals Collected on the Field

The time history file array for one pass over paved road is shown in Fig. 8. This figure shows the displacement signal of the four actuators, at the rear right axis, rear left, front right, and front left, respectively, with the vehicle in Std C.

The error curve for the four actuators in relation to the acquired road signal is shown in Fig. 9. A gradual decrease in the value of the error (%) is noted as the iterations are performed. This value goes from ±50% in the first iteration to ±8% after eleven iterations.

3.3 Durability Test

During the 12 000 km of the durability test, there was no evidence of ruptures that might significantly compromise the

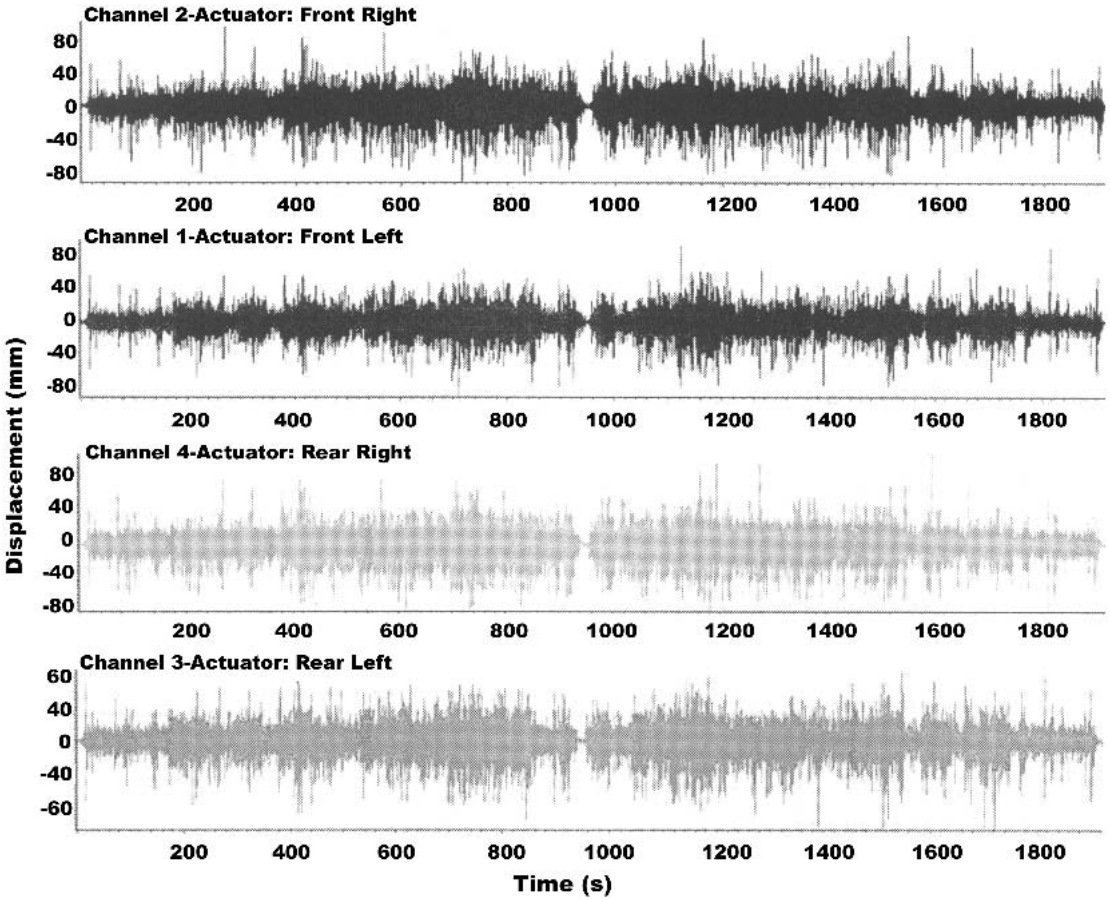

Fig. 8 Wheel transducer displacements

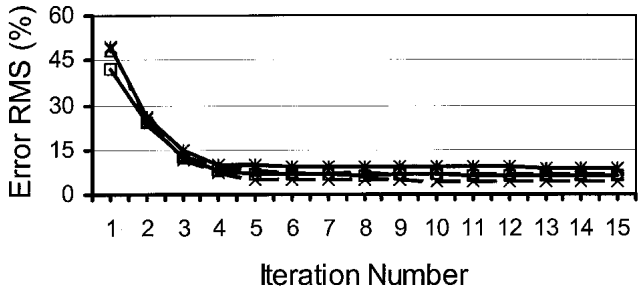

Fig. 9 Iteration convergence curves

integrity and the safety of the vehicle, as made evident in the finite element analysis.

The acquisition of signals of microstrains was made at several values of kilometers encompassing paved and land surface stretches, with the vehicle loaded and empty. When this step was finished, the Von Mises stress was calculated, with the purpose of verifying the most critical condition to which the vehicle is submitted.

A comparison of the values obtained shows that the highest stress values are on the paved roads with the loaded vehicle, as shown in Table 9.

Microstrain values obtained from the rosettes located at nodes A and B on the passenger side for paved stretch are shown in Fig. 10 and 11. These values are typical of those representing the driver side and land surface.

3.4 Torsion Test

First at all, a rigid rear and front suspension with welded dampers was prepared for this test. The purpose was to simulate the body shell with loading Std C, which was the most critical condition during stress acquisition. Thus, a body-in-white was mounted on the test setup and a torque of 200 kgm is applied. The results of this experiment are shown in Table 10.

The same experiment was performed for the full vehicle body shell. The results are shown in Table 11.

The microstrain values obtained from the rosettes located on the passenger side with a full vehicle body shell are shown in Fig. 12 and 13.

4. Discussion of the Results

4.1 Finite Element Analysis and Experimental Analysis

A comparison between the results obtained from finite element analysis and those obtained experimentally, both using a body-in-white shell, is shown in Table 12.

It is observed that the values obtained from both meth-

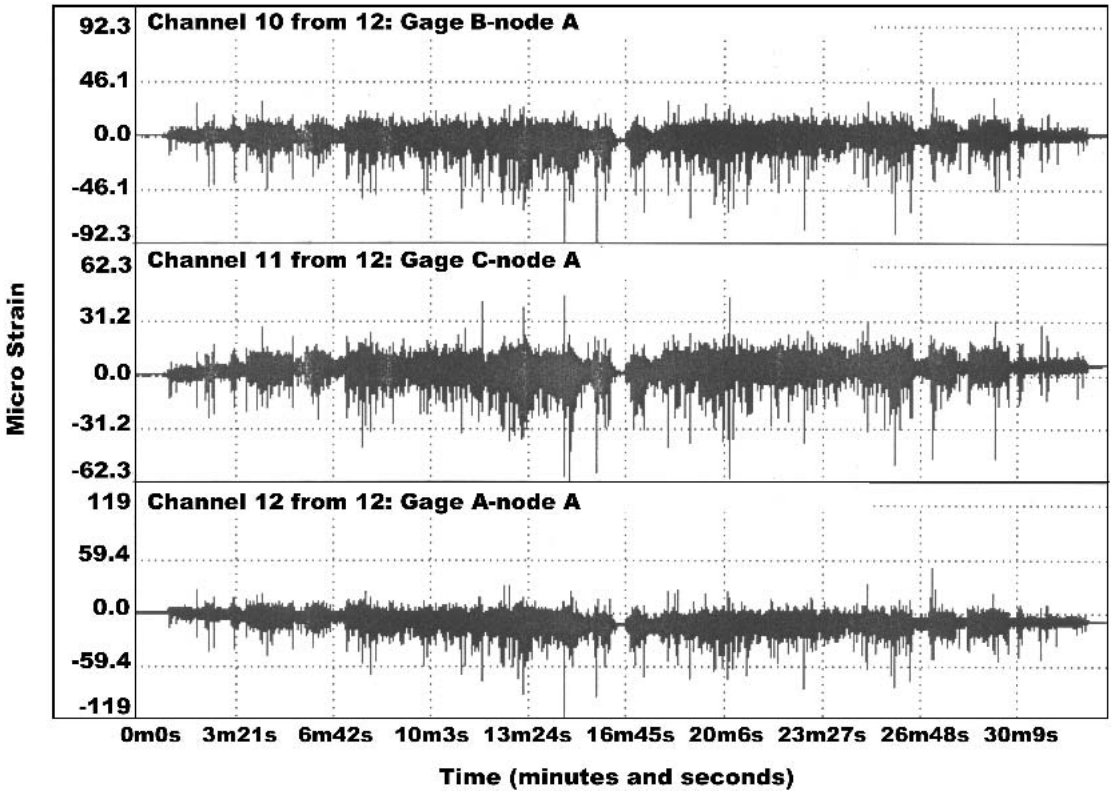

Fig. 10 Microstrain values: Rosette on node A passenger side, Paved

ods are quite similar. The results of finite element analysis were very important to determine the region for fixing the rosettes, as well as during the selection of the type of rosette used.

In this table it is also shown that the variation between stress values in the same nodes, but on opposite sides was about ±4% between the sides of node B and ±19% between the sides of node A. A reason for this discrepancy may be the asymmetry of the internal components of the body shell as sheet reinforcements and weld spots. This is more evident on the region of node A since this node is located near a reinforcement plate of the instrument panel, which has a highly asymmetric form.

4.2 Cumulative Damage Determination

The methodology of cycle counting using rain flow and the calculation of cumulative damage became a fundamental tool to estimate a correlation between durability test damage and torsion test. This correlation is, in principle, based on the comparison of the damage generated in a cycle of torsion of the fully vehicle body shell and a stretch of 110 km of durability. This stretch is divided into 2/3 stone pavement and 1/3 land surface, as the kilometer distribution principle of the durability test.

The rain flow was calculated considering the values of Von Mises alternated stress and mean stress, Eq 3 and 4, respectively. The cumulative damage was calculated using Miner's rule (Eq 1). The values obtained for the cumulative damage for a rosette positioned on the node A, at the passenger side, are shown in Tables 13, 14, and 15.

Table 9 Von Mises Stress Data Acquisition

Rosettes Location	Driver Side				Passenger Side			
Von Mises	Node B		Node A		Node B		Node A	
Stress, MPa	Max	RMS	Max.	RMS	Max	RMS	Max	RMS
Paved								
Vehicle Std C	61.8	8.5	42.33	2.8	41.95	2.45	27.49	2.61
Land Surface								
Vehicle Std C	59.76	9.07	36.93	3.42	31.82	2.61	22.4	2.05
Paved								
Vehicle Std B	48.87	9.71	28.78	3.14	26.11	2.22	14.07	2.44
Land Surface								
Vehicle Std B	62.83	9.94	18.14	2.36	25.94	2.16	15.31	2.29

For each alternating and mean stress pair, the equivalent alternating stress to a zero mean stress, corresponding to the same life [$\sigma_{N(0)}$], was calculated using Goodman method (Eq 2). As a example, it was taken the first line of Table 13 with stress amplitude ($2\sigma_a$ = 20.63 MPa) and mean stress (σ_m = 10.78 MPa). Using Eq 2 to calculate $\sigma_{N(0)}$ leads to

$$\sigma_{N(0)} = (20.63/2) \cdot 270 / (270 - 10.78) = 10.74 \text{ MPa}$$

In these calculations, it was considered that σ_r = 270 MPa based on the most critical situation of the tensile strength of the material, according to Table 2.

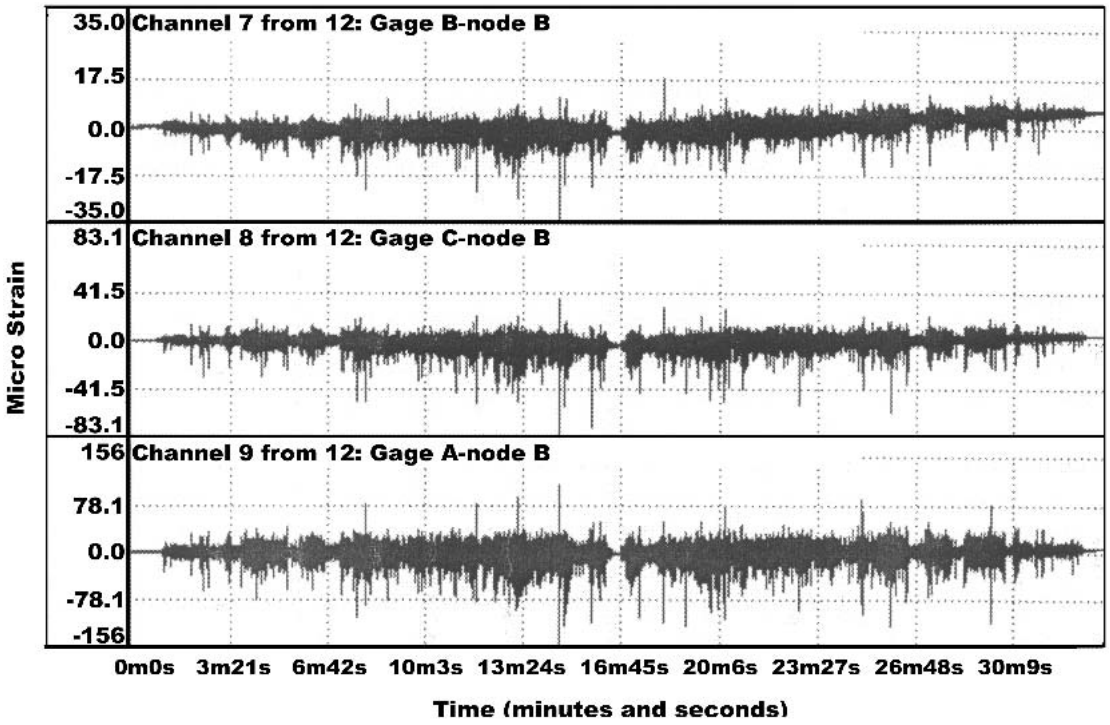

Fig. 11 Microstrain values: Rosette on node B passenger side, Paved

Table 10 Body-In-White Torsion Test Results

	Von Mises Stress, MPa
Gauge Location/results	Experimental analysis
Node B, driver side	16.4
Node B, passenger side	17.06
Node A, driver side	45.26
Node A, passenger side	36.31

Table 11 Fully Vehicle Body Shell Torsion Results

	Von Mises Stress, MPa
Gauge Location/Results	Experimental analysis
Node B, driver side	5.39
Node B, passenger side	4.75
Node A, driver side	12.92
Node A, passenger side	8.17

To determine the life N, it is necessary to estimate the S-N Curve equation:

$$S_N = aN^b \quad \text{(Eq 5)}$$

The parameters a and b were empirically obtained by estimating the fatigue limit Se = 84.8 MPa, taking into account correction factors equal to 0.6279. A reliability of 90% for the fatigue resistance limit was used. This estimate becomes necessary, since the S-N curve for the body shell was not available. A S-N curve is a locus of all points of equal fatigue damage. Its use here is to estimate comparative damage imposed on the shell nodes. Thus the exact slope is not essential, as long as the same slope is used for all of the estimates. The life N for each alternating stress can be then determined using Eq 5:

$10.74 = 684.9\ N^{-0.15}$, then: $N = 1.07 \times 10^{12}$ cycles.

Finally, the cumulative partial damage was determined using the Miner rule:

$$D = 1/1.07 \times 10^{12}$$

$$D = 9.32 \times 10^{-13}$$

To calculate the cumulative total damage of the durability test, the kilometer distribution of the road simulator was taken as a reference (Fig. 6). Each test stretch (loaded and empty) was divided by 110 km with the purpose of finding a multiplying factor for the cumulative damage from Tables 13 and 14. Taking as a reference the total cumulative damage for 110 km on Table 13, and the first loaded stretch of Fig. 6, the following was obtained:
First loaded stretch = 615 km
Multiplier factor = 615 km/110 km = 5.59
Total damage (Table 13) $= 1.74 \times 10^{-11} \times 5.59 = 9.73 \times 10^{-11}$

The cumulative damage values for 12 000 km with the vehicle, loaded and empty, on each node of the body shell are shown in Tables 16 and 17.

The total damage was obtained for the 12,000 km durability test by adding up total damage for the vehicle: loaded, empty, each node of the body shell. Results are shown in Table 18.

It can be verified from Table 18 that the maximum cumu-

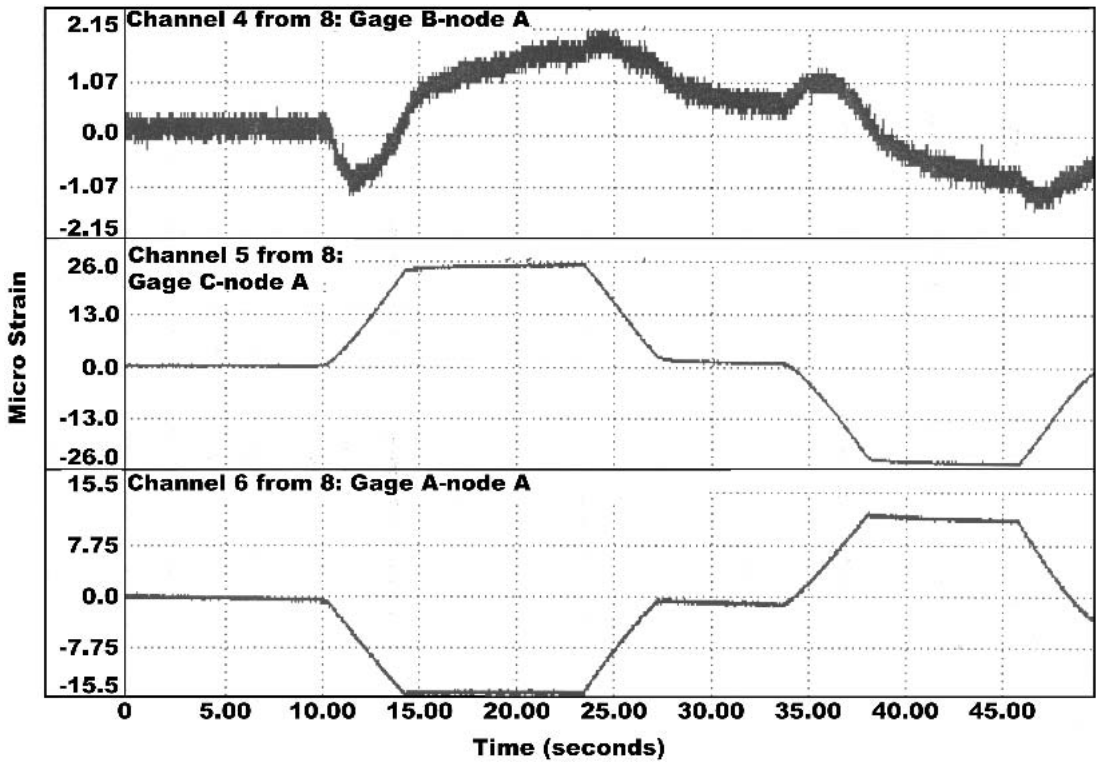

Fig. 12 Microstrain values: Rosette on node A passenger side, Full Vehicle

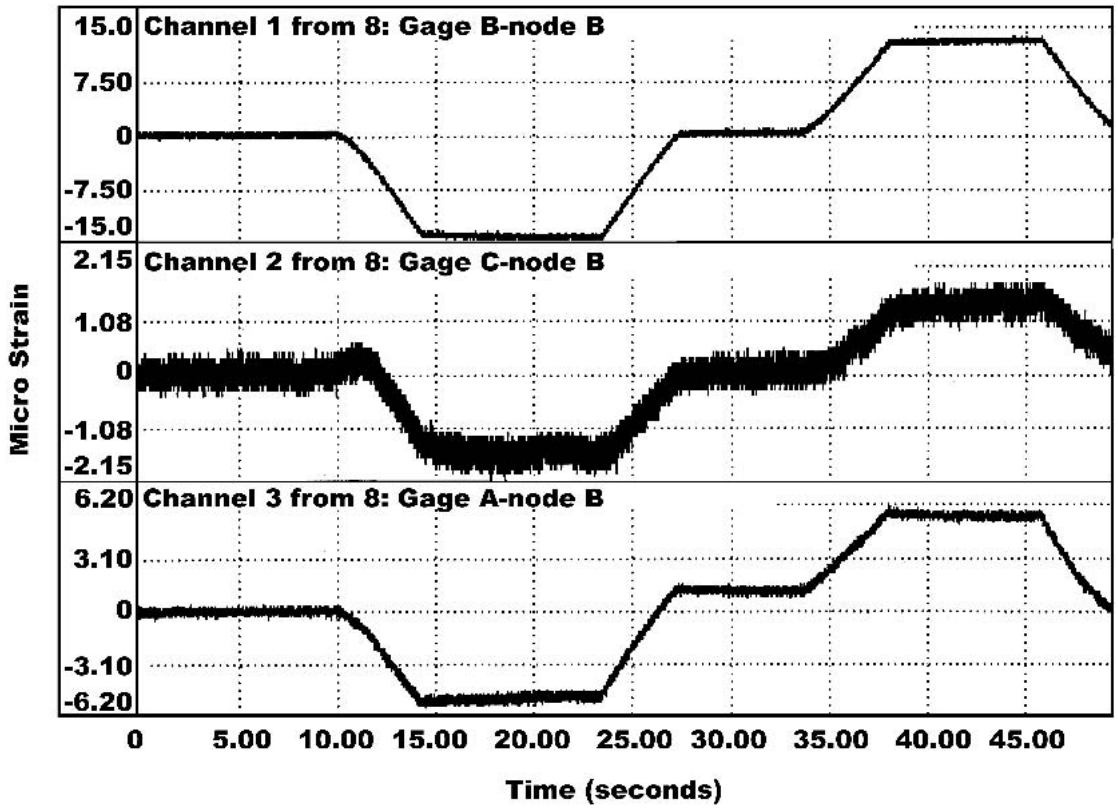

Fig. 13 Microstrain values: Rosette on node B passenger side, Full Vehicle

Table 12 Comparison Between Finite Element Analysis and Experimental Results

	Von Mises Stresses, MPa	
Gage location/results	Finite element	Experiment
Node B - Driver side	17.8-26.7	16.4
Node B - Passenger side		17.06
Node A - Driver side	35.5-44.4	45.26
Node A - Passenger side		36.31

Table 13 Cumulative Damage for 110 km With Loaded Vehicle

σ_a, MPa	σ_m, MPa	$\sigma_{N(0)}$, MPa	Life N, Cycles	Cycles Number, n	Damage
20.63	10.78	10.74	1.07E + 12	1	9.32E – 13
19.69	0.94	9.88	1.88E + 12	3	1.60E – 12
19.69	0.00	9.84	1.92E + 12	1	5.21E – 13
18.75	20.16	10.13	1.58E + 12	1	6.31E – 13
18.75	0.47	9.39	2.63E + 12	4	1.52E – 12
17.81	0.94	8.94	3.65E + 12	3	8.21E – 13
…	…	…	…	…	…
0.94	1.88	0.47	1.20E + 21	20 194	1.69E – 17
0.94	0.94	0.47	1.22E + 21	17 441	1.42E – 17
0.94	0.00	0.47	1.25E + 21	7 774	6.20E – 18
Total Damage					1.74E – 11

Table 14 Cumulative Damage for 110 km With Empty Vehicle

σ_a, MPa	σ_m, MPa	$\sigma_{N(0)}$, MPa	Life N, Cycles	Cycles Number, n	Damage
13.75	7.19	7.06	1.75×10^{13}	1	5.70×10^{-14}
13.13	0.63	6.58	2.82×10^{13}	1	3.55×10^{-14}
12.50	4.06	6.35	3.58×10^{13}	1	2.79×10^{-14}
12.50	0.31	6.26	3.94×10^{13}	4	1.02×10^{-14}
11.88	0.63	5.95	5.50×10^{13}	3	5.46×10^{-14}
11.88	0.00	5.94	5.58×10^{13}	1	1.79×10^{-14}
11.25	0.31	5.63	7.94×10^{13}	4	5.04×10^{-14}
10.63	3.75	5.39	1.15×10^{14}	1	9.37×10^{-14}
10.63	0.63	5.32	1.15×10^{14}	2	1.73×10^{-14}
…	…	…	…	…	…
0.63	1.25	0.31	1.20×10^{21}	20 194	7.66×10^{-19}
0.63	0.63	0.31	1.22×10^{21}	17 441	2.75×10^{-19}
0.63	0.00	0.31	1.25×10^{21}	7 774	7.80×10^{-19}
Total Damage					8.48×10^{-13}

lative damage was for node B on driver side. This value of damage is associated to the number of cycles (n) related to the maximum stress amplitude value in Table 15. The purpose is to calculate a total number of cycles (N) for the fatigue of the body shell in the torsion test. The number of cycles to be obtained is calculated through Miner's equation:

$N = 1/1.73 \times 10^{-6}$; thus $N = 5.78 \times 10^5$ cycles.

From Eq. 5, the value for stress $\sigma_{N(0)}$, with $\sigma_m = 0$ and $N = 5.78 \times 10^5$ cycles, for the node B on the drivers side can be determined:

Table 15 Cumulative Damage for 1 Torsion Cycle

σ_a, MPa	σ_m, MPa	$\sigma_{N(0)}$, MPa	Life N, Cycles	Cycles Number, n	Damage
5.63	2.91	2.84	7.57×10^{15}	1	1.32×10^{-16}
5.25	2.91	2.65	1.20×10^{16}	1	8.34×10^{-17}
Total Damage					8.34×10^{-17}

Table 16 Total Cumulative Damage for Durability Tests With Loaded Vehicle

Gage Position	Node B Driver Side	Node B Passenger Side	Node A Driver Side	Node A Passenger Side
Multiplier for 110 km	1.74×10^{-11}	6.15×10^{-10}	6.01×10^{-10}	1.74×10^{-11}
5.59	9.73×10^{-11}	3.44×10^{-9}	3.36×10^{-9}	9.73×10^{-11}
18.91	3.29×10^{-10}	1.16×10^{-8}	1.14×10^{-8}	3.29×10^{-10}
30.05	5.23×10^{-10}	1.85×10^{-8}	1.81×10^{-8}	5.23×10^{-10}
Total Damage	9.49×10^{-10}	3.35×10^{-8}	3.28×10^{-8}	9.49×10^{-10}

Table 17 Total Cumulative Damage for Durability Test With Empty Vehicle

Gage Position	Node B Driver Side	Node B Passenger Side	Node A Driver Side	Node A Passenger Side
Multiplier for 110 km	3.17×10^{-8}	9.19×10^{-12}	1.03×10^{-11}	8.48×10^{-13}
6.27	1.99×10^{-7}	5.76×10^{-11}	6.46×10^{-11}	5.32×10^{-12}
23.63	7.49×10^{-7}	2.17×10^{-10}	2.43×10^{-10}	2.00×10^{-11}
20.91	6.63×10^{-7}	1.92×10^{-10}	2.15×10^{-10}	1.77×10^{-11}
3.73	1.18×10^{-7}	3.43×10^{-11}	3.84×10^{-11}	3.16×10^{-12}
Total Damage	1.73×10^{-6}	5.01×10^{-10}	5.62×10^{-10}	4.62×10^{-11}

Table 18 Total Cumulative Damage for a Durability Test

Damage	Node B Driver Side	Node B Passenger Side	Node A Driver Side	Node A Passenger Side
Empty	1.73×10^{-6}	5.01×10^{-10}	5.62×10^{-10}	4.62×10^{-11}
Loaded	9.49×10^{-10}	3.35×10^{-8}	3.28×10^{-8}	9.49×10^{-10}
Total	1.73×10^{-6}	3.40×10^{-8}	3.34×10^{-8}	9.95×10^{-10}

$\sigma_{N(0)} = 684.9(5.78 \times 10^5)^{-0.15} \rightarrow \sigma_N = 93.91$ MPa.

Supposing that the torsion test will be performed 24 hours a day, with frequency $f = 0.5$ Hz, 14 days will be necessary to cause the failure of the body shell. This represents a difference of 7 days in development, since the durability test lasts about 20 days.

5. Conclusions

From the results and discussions presented above, it can be concluded that

- The finite elements analysis proved to be an important tool in the process of validation of the experimental data.
- The acquisition of stress signals on the road showed that the higher values were found during the stretch of paving with loaded vehicle.
- From the damage caused in durability test after 12,000 km, a number of cycles $N = 5.78 \times 10^5$ was estimated to cause the same fatigue damage of the body shell in the torsion test.
- It is necessary to confirm the results of stress σ_N and the number of cycles (N) estimated for the body shell fatigue test in the torsion test setup. For this confirmation, one should take into account a high level of reliability of the results obtained through the Weibull distribution and Success Run.
- The purpose for using a torsion fatigue experiment is not to eliminate the road simulator test, since it tests many other components of the vehicle. The purpose is to reduce costs, since eventual ruptures of the body shell before the durability test in the simulator can be avoided.

References

1. X. Yang, N. Li, Z. Jin, and T. Wang: "A Continuous Low Cycle Fatigue Damage Model and Its Application In Engineering Materials," *Int. J. Fatigue,* 1997, *9*(10), pp. 687-92.
2. A. Fatemi and L. Yang: "Cumulative Fatigue Damage and Life Prediction Theories: A Survey of the State of the Art for Homogeneous Materials," *Int. J. Fatigue,* 1998, *20*(1), pp. 9-34.
3. N.E. Dowling, "Estimation and Correlation of Fatigue Lives for Random Loading," *Int. J. Fatigue*, 1988, *10*(3), pp. 179-85.
4. D.L. DuQuesnay, M.A. Pompetzki, and T.H. Topper: "Fatigue Life Prediction for Variable Amplitude Strain Histories, Fatigue Research, and Applications," SAE SP-1009, Warrendale, PA, 1993.
5. R.E. Canfield and M.A. Villaire: "The Development of Accelerated Component Durability Test Cycles Using Fatigue Sensitive Editing Techniques," SAE World Congress, Paper No. 920660, 1992, pp. 69-79.
6. R.W. Landgraf and S. Thangjitham, "Reliability Analysis of an Automotive Wheel Assembly," SAE World Congress, Paper No. 930406, 1993, pp. 225-35.
7. G.E. Leese and R.L. Mullin, "The Role of Fatigue Analysis in the Vehicle Test Simulation Laboratory, Recent Development in Fatigue Technology," SAE Paper No. 910166, 1991, pp. 57-68.
8. P. Cicala and L. Garro: *Analisi delle Sollecitazioni dei Giunti di Carrozzeria di un Veicolo*, Fiat Auto Spa, Torino, Italy, *343,* pp. 166-69 (In Italian).
9. J. Collins: *Failure of Materials in Mechanical Design—Analysis, Prediction and Prevention,* 2nd ed., John Wiley & Sons, New York, NY, 1993.
10. Anon: *SAE Fatigue Design Handbook*, 3rd ed., R.C. Rice, ed., Society of Automotive Engineers, Warrendale, PA, 1997, AE-22.
11. D. Shutz and H. Lowak: "The Application of the Standardized Test Program for the Fatigue Life Estimation of Fighter Wing Components Falstaff (Part IV)," *Proceedings of the 8th ICAF Symposium on Problems with Fatigue in Aircraft*, ICAF, Lausanne, Switzerland, June 2-5, 1975, pp. 3.64/1-3.64/22.
12. Anon: "Lamieri e Nastri di Acciaio non Legato, Laminati a Freddo, per Imbutitura e Piegamento a Freddo," *Norma Materiali,* 12th ed., Fiat Auto Spa, Torino, Italy, 1996, No. 52806, p.7 (In Italian).
13. Anon: Model 320 Tire Coupled Road Simulator, the MTS "Four Poster", MTS Systems Corporation, Minneapolis, MN, 1996, p. 15.